



Article

Probing the Kinetic and Thermodynamic Fingerprints of Anti-EGF Nanobodies by Surface Plasmon Resonance

Salvador Guardiola ¹ , Monica Varese ¹, Marta Taulés ², Mireia Díaz-Lobo ³, Jesús García ¹ and Ernest Giralt ^{1,4,*}

¹ Institute for Research in Biomedicine (IRB Barcelona), The Barcelona Institute of Science and Technology (BIST), 08028 Barcelona, Spain; salvador.guardiola@irbbarcelona.org (S.G.); monica.varese@irbbarcelona.org (M.V.); jesus.garcia@irbbarcelona.org (J.G.)

² Scientific and Technological Centres (CCiT-UB), Molecular Interactions, University of Barcelona, 08028 Barcelona, Spain; marta@ccit.ub.edu

³ Mass Spectrometry and Proteomics Core Facility, Institute for Research in Biomedicine (IRB Barcelona), The Barcelona Institute of Science and Technology (BIST), 08028 Barcelona, Spain; mireia.diaz@irbbarcelona.org

⁴ Department of Inorganic and Organic Chemistry, University of Barcelona, 08028 Barcelona, Spain

* Correspondence: ernest.giralt@irbbarcelona.org

Received: 2 June 2020; Accepted: 24 June 2020; Published: 26 June 2020



Abstract: Despite the widespread use of antibodies in clinical applications, the precise molecular mechanisms underlying antibody–antigen (Ab–Ag) interactions are often poorly understood. In this study, we exploit the technical features of a typical surface plasmon resonance (SPR) biosensor to dissect the kinetic and thermodynamic components that govern the binding of single-domain Ab or nanobodies to their target antigen, epidermal growth factor (EGF), a key oncogenic protein that is involved in tumour progression. By carefully tuning the experimental conditions and transforming the kinetic data into equilibrium constants, we reveal the complete picture of binding thermodynamics, including the energetics of the complex-formation transition state. This approach, performed using an experimentally simple and high-throughput setup, is expected to facilitate mechanistic studies of Ab-based therapies and, importantly, promote the rational development of new biological drugs with suitable properties.

Keywords: nanobodies; SPR; biophysics; thermodynamics; molecular recognition; EGF; antibody–antigen (Ag–Ab) interactions

1. Introduction

Antibody–antigen (Ab–Ag) interactions are one of the most relevant classes of protein-mediated molecular recognition processes. They have been selected during millions of years of evolution for their ability to bind with high specificity and affinity to a wide variety of antigenic molecules [1,2]. From a pharmaceutical perspective, the last decade has witnessed an explosion in the use of Ab for imaging [3], drug conjugation [4], diagnostic [5] and therapeutic [6] purposes, among many others. Although the key strengths of Abs are widely recognised in terms of affinity, specificity and biochemical stability, full-length monoclonal antibodies (mAbs) suffer from some limitations when it comes to their clinical development, such as undesired Fc-mediated cytotoxicity, poor penetration in target tissues, aggregation and stability problems, low batch-to-batch reproducibility, and elevated manufacturing costs, among others [7]. To overcome these issues, a variety of Ab formats have been developed and optimised in recent years, thanks to the remarkable progress achieved in protein engineering

and in vitro display methods [8,9]. Among these Ab formats, camelid-derived single-domain Abs, also known as VHHs or nanobodies, are the smallest Ag-binding proteins found in nature and have attracted great interest for biotechnological and pharmaceutical applications [10]. Unlike conventional Abs, nanobodies are formed by a single chain of only ~14 kDa and they can be readily expressed in recombinant bacteria with high yields [11]. Despite their small size, being one-tenth of a standard IgG antibody, nanobodies can engage their targets with similar affinities and specificity to full-length Abs. In addition, compared to mAb, they have a longer variable CDR3 loop, which forms part of a bulging interface that is ideally suited for targeting cavities, grooves and flexible epitopes [12].

Despite the undeniable progress achieved with the development of therapeutic Abs, there are relatively few studies shedding light on the kinetics and thermodynamics that drive antigen recognition [13–15]. Moreover, some of these studies have been performed with model systems consisting of full-length Abs that recognise small-molecule antigens [16,17]. On the contrary, the analysis of pharmacologically relevant Ab–Ag interactions, at the mechanistic level, is of utmost importance for the success of therapeutic antibodies during preclinical stages of development.

Protein–protein interactions in general, and antibody–antigen interactions in particular, can be characterised at several quantitative levels. One of the simplest descriptors is defined by the dissociation constant (K_D), a measure of the strength of the interaction at equilibrium. The K_D may be further resolved into its kinetic descriptors, namely the association (k_{on}) and dissociation (k_{off}) rate constants of Equation (1), which give information about the rate of complex formation and its stability

$$K_D = \frac{k_{off}}{k_{on}} = \frac{1}{K_A} \quad (1)$$

Despite being widely used in drug discovery projects, kinetic information alone is insufficient to fully assess the mechanism of binding interactions [18]. In contrast, thermodynamic parameters define the state at equilibrium in which Gibbs free energy (G) is the lowest. Large negative changes in ΔG upon binding define a strong molecular interaction. In fact, the relationship between ΔG and the equilibrium constant (K_D) is mathematically described by the Gibbs equation Equation (2). ΔG can be further decomposed into its enthalpy (ΔH) and entropy (ΔS) components

$$\Delta G^\circ = RT \ln K_D = \Delta H^\circ - T \Delta S^\circ \quad (2)$$

In Ab–Ag interactions, binding enthalpy ΔH is associated mainly with the strength and specificity of the interaction contacts. These are usually related to hydrogen bonds and electrostatic interactions, although solvent reorganization and conformational change might also have an influence on ΔH . On the other hand, binding entropy (ΔS) reflects the degree of order and disorder of the system and is often linked to the behaviour of surface-bound water molecules, as well as changes in the conformational flexibility of the binding partners. Finally, the temperature dependence of ΔH and ΔS can be defined by changes in the systemic heat capacity (ΔC_p), as comprised in the van't Hoff equation Equation (3), where the association constant (K_A) is the inverse of K_D

$$\ln K_A = \frac{\Delta H^\circ T^\circ}{RT} + \frac{\Delta S^\circ T^\circ}{R} + \frac{\Delta C_p}{R} \left[\left(\frac{T - T^\circ}{T} \right) - \ln \left(\frac{T}{T^\circ} \right) \right] \quad (3)$$

Thus, a quantitative assessment of Ab–Ag interactions requires the determination of changes in all thermodynamic parameters, including ΔG , ΔH , ΔS and ΔC_p . The heat effects (ΔH) of an interaction can be directly measured using isothermal titration calorimetry. However, providing that immobilisation of the protein does not affect its bioactivity, kinetic and thermodynamic parameters can be also calculated from the same experimental dataset using a biosensor technique such as surface plasmon resonance (SPR). Compared to calorimetry measurements, the SPR analysis comes at a much lower time and protein consumption cost.

Our group recently reported the discovery of nanobodies against epidermal growth factor (EGF) [19], a key oncogenic protein involved in the progression of epidermal-based tumours, such as those of the lung, skin and colon, among others [20]. In the present study, we have leveraged the potential of SPR for accurately measuring non-covalent interactions at different temperatures and analyte concentrations to study the kinetics and thermodynamics of two of our leading anti-EGF targeted nanobodies (Nb1 and Nb6). Our analysis thus provides a valuable case study of the distinct molecular forces that drive Ag-Ab binding events, with a special emphasis on the behaviour of single-chain Ab or nanobodies.

2. Results

To probe the interactions of Nb1 and Nb6 with their target antigen, we recombinantly expressed human EGF [21] and immobilised it by amine coupling on a CM5 sensor chip. Although different ligand orientations might occur, the three-dimensional dextran hydrogel layer of the chip minimises steric occlusion of the protein. Furthermore, EGF has been shown to maintain its bioactivity intact in amine-coupling immobilisation experiments on SPR chips [22]. Low immobilisation levels of ligand were prioritised (50 and 100 RU, on two different channels) to avoid mass transfer limitations and re-binding artefacts, as well as unspecific non 1:1 interactions [23]. When injected at increasing concentrations, both nanobodies produced, as expected, concentration-dependent SPR sensorgrams and signal saturation at the highest concentrations (Figure 1). We calculated the equilibrium dissociation constants (K_D) at 25 °C, by either (I) plotting the level of steady-state binding for each concentration (i.e., equilibrium fitting, Figure S1); or (II) fitting the association and dissociation signals separately, as a function of time, to a given interaction model (i.e., kinetic fitting, Figure 1).

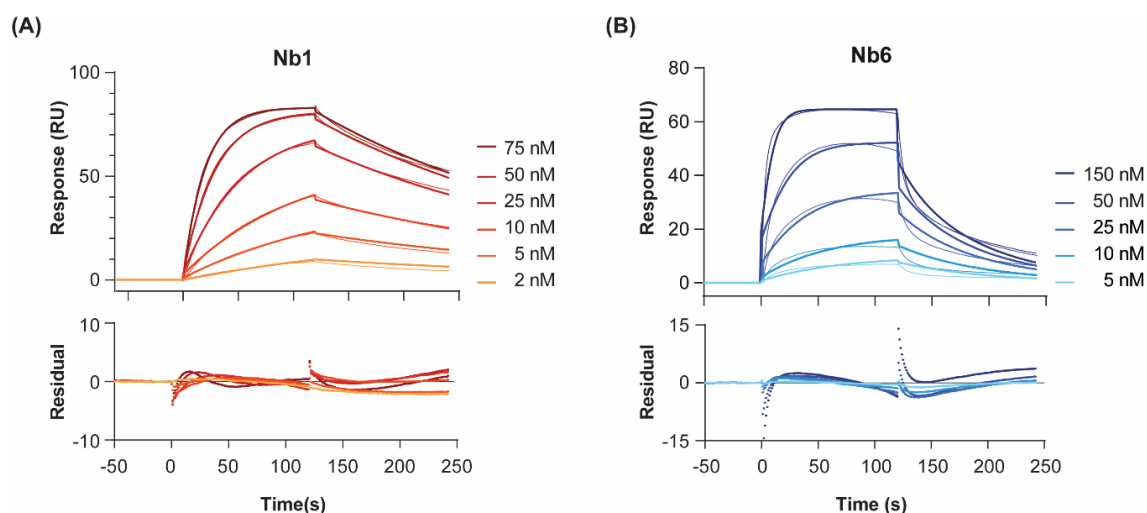


Figure 1. Binding kinetics of Nb1 (A) and Nb6 (B) to EGF at 25 °C. Nanobodies were injected at increasing concentrations over immobilised EGF, and the association and dissociation phases of all injections were fitted to a 1:1 Langmuir binding model. Two different surface densities were used for k_{on} , k_{off} and K_D determination, with the corresponding background responses subtracted. Double-referenced sensorgrams for the highest density channel are shown here. Experiments were performed in duplicates. Residual errors from the fits are shown in the bottom panels.

For both nanobodies binding to EGF, a 1:1 Langmuir interaction model had been previously confirmed by isothermal calorimetry [19]. In agreement, a 1:1 kinetic model provided a close fit to the experimental data, as shown by the low chi-square values ($\chi^2 = 0.8\text{--}2.9$). Regarding the association step, both nanobodies showed fast on-rates (6 and $8 \times 10^5 \text{ M}^{-1} \text{ s}^{-1}$ for Nb1 and Nb6, respectively). On the other hand, the dissociation phase was significantly slower for Nb1. In general, slow binders such as Nb1 reach the SPR steady state (i.e., the timepoint at which the net rate of complex formation is

zero) only after very long injection times. In the case of Nb1, it took 300 s to reach 90% of equilibrium at a concentration C equal to its K_D (6 nM). Since experimental injection times in SPR are typically shorter (in our case, 120 s), more reliable K_D values are measured by kinetic fitting, which is independent of steady-state levels. It should be noted that these K_D values are, to some extent, lower than those we previously reported using a different biosensor method, namely surface acoustic wave (SAW) [19]. However, in the SAW technique, the ligand EGF was immobilised at higher densities using a different surface chemistry (alkanethiol monolayer, versus the three-dimensional dextran layer used here for SPR), which could result in mass-transport-limited kinetics, especially for the fastest binders. These differences might explain why, while the affinity (K_D) constants are comparable, SAW-derived on- and off-rates were about an order of magnitude slower than those calculated here by SPR.

To analyse the variation of kinetics with temperature in more detail, we performed SPR experiments at temperatures ranging from 9 to 37 °C (Figure 2). Binding dissociation followed first-order kinetics at all temperatures, as shown by the nearly linear logarithmic plots of the dissociation phases (Figure S2). A 1:1 binding model was applied to extract k_{on} and k_{off} kinetic constants for each analyte concentration and temperature. The resulting fits, plotted as coloured lines for a single Nb concentration (70 nM) over a range of temperatures (Figure 2A,B), closely described the experimental data. As expected, the kinetics slowed dramatically for both Nbs when the temperature was decreased from room temperature to 9 °C. In contrast, faster association and dissociation sensorgrams were observed with heating to human physiological temperature (37 °C). This effect was more pronounced for the dissociation rate, which translated into an overall drop in the half-life of the complex at the highest temperatures.

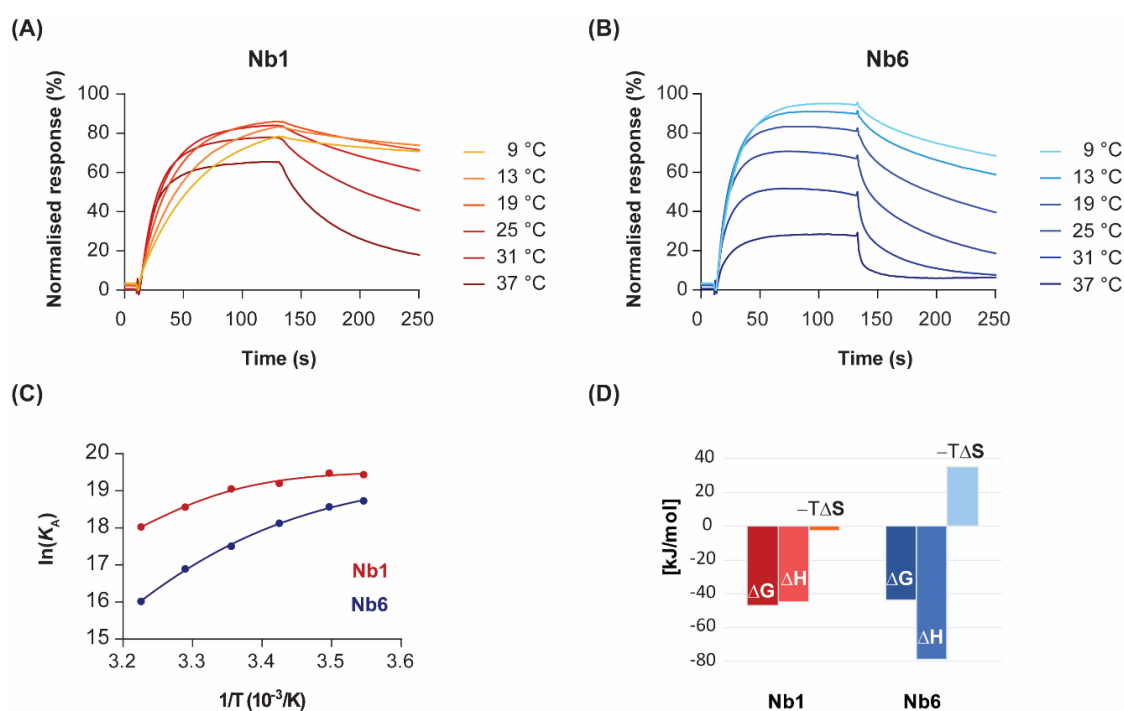


Figure 2. Temperature dependence of binding kinetics and thermodynamic characterisation. Nb1 (A) and Nb6 (B) were injected over immobilised EGF at the indicated temperatures. For clarity, only sensorgrams of a single analyte concentration (70 nM) are shown. (C) Van't Hoff plots representing the variation of the equilibrium association constants (K_A) with the inverse of temperature. Data points were fitted to a second-order polynomial equation from which ΔG , ΔH , ΔS and ΔC_p values were determined, following Equation (3). (D) Enthalpy (ΔH) and entropy ($-T\Delta S$) contributions to the free energy of binding (ΔG) for each Nb at 25 °C.

By representing the change in the equilibrium association constant (K_A) as a function of temperature, in what is known as the van't Hoff plot Equation (3), one can gain mathematical access to the thermodynamics of the interaction. In the absence of heat capacity changes, van't Hoff plots should be linear and thus discriminate between two terms: an enthalpic contribution that is linear in the inverse of temperature ($1/T$), and a temperature-independent entropic contribution. However, significant curvature in the van't Hoff plots was observed for both nanobodies at temperatures ranging from 9 to 37 °C (Figure 2C). Although there is always a risk of model overfitting to non-ideal SPR data, the residual values of our global kinetic fitting are very small (see Figure 1, bottom panel). Thus, the lack of linearity in the van't Hoff plots reveals instead non-zero heat capacity changes (ΔC_p) for the interactions. The physical reason for the temperature dependence of ΔH is attributed to changes in solvent-accessible surface areas that are buried in the binding process [24]. In particular, the convex shape of the van't Hoff plots is indicative of negative ΔC_p , which might result from the burial of hydrophobic protein patches upon complex formation.

Non-linear regression using Taylor's polynomials allowed the determination of the main thermodynamic parameters for each nanobody (Figure 2D and Table 1). The relative energetic contributions (ΔH and ΔS) are in good agreement with calorimetry data [19]. The binding of Nb1 to EGF was driven by both entropy and enthalpy components, although there was a strong temperature-dependence for ΔH . Since the tangent to the curve at any point of the van't Hoff plot is ΔH at that precise temperature, the decrease in the Nb1 binding enthalpy is especially evident at lower temperatures. In fact, the binding of Nb1 is purely entropy-driven below 10 °C. In a similar fashion, Nb6 showed a convex van't Hoff plot indicative of a large negative ΔC_p value (Table 1). However, in contrast to Nb1, Nb6 paid a significant entropic penalty for binding its antigen, which was largely compensated by a favourable change in ΔH . As shown here, the negative ΔS is a common feature among most antibodies, since they possess a certain degree of flexibility in the CDR loops that form the antigen-binding site [25]. Besides being attributed to a decreased conformational freedom of the complex, the entropic penalty of Nb6 can also be interpreted in terms of binding to a more hydrophilic epitope on EGF than that of Nb1, thus releasing fewer water molecules into the bulk solvent.

According to transition state theory [26], the temperature dependence of k_{on} and k_{off} allows analysis of the thermodynamics of activation to form the transition state via the Eyring equation

$$\ln\left(\frac{kh}{k_B T}\right) = \frac{\Delta H^\ddagger T^0}{RT} + \frac{\Delta S^\ddagger T^0}{R} + \frac{\Delta C_p^\ddagger}{R} \left[\left(\frac{T - T^0}{T} \right) - \ln\left(\frac{T}{T^0} \right) \right] \quad (4)$$

In a reversible binding process, such as the one studied here, the [EGF-Nb] ‡ transition state is the high energy state along the binding pathway from free species to complex, which is also visited on the dissociation from the complex to the free species. The thermodynamic approach described herein provides additional information to the classical ITC studies, since SPR monitors the physical association and dissociation of the two molecular species, whereas in calorimetric assays the total heat of the interaction—including heat of dilution or mixing—is measured.

In its graphical representation, it appears that the Eyring plot for Nb1 association (k_{on}) is linear but significantly dependent on temperature, corresponding to a large activation enthalpy ΔH^\ddagger (Figure 3A). The dissociation Eyring plot (representing k_{off}) reveals the curvature that is also present in the van't Hoff plot (Figure 2C), as discussed above. In contrast, for Nb6, both association and dissociation Eyring plots are non-linear (Figure 3B,C). The solution of Eyring's equation, via Taylor's series for the non-linear models provides the transition state thermodynamic parameters (denoted by a superscript "‡").

As shown in Figure 3D, both nanobodies must overcome a significant free energy barrier in order to bind the target. Although enthalpy drives complex formation in both cases, the transition state of Nb6 is characterised by a decrease in the association entropy, which indicates that a reduction in conformational flexibility and structural reordering in the interface is required for binding. This behaviour is in striking contrast to typical protein–protein interactions, in which the entropic changes are typically favourable and thus contribute to an increased affinity [27].

Table 1. Summary of all kinetic and thermodynamic constants.

Id	k_{on} ($M^{-1} s^{-1}$)	k_{off} (s^{-1})	K_D^a (nM)	K_D^b (nM)	ΔG^o ($kJ mol^{-1}$)	ΔH^o ($kJ mol^{-1}$)	$-T\Delta S^o$ ($kJ mol^{-1}$)	ΔC_p^o ($kJ K^{-1} mol^{-1}$)
Nb1-EGF	$6.6 \times 10^5 \pm 5 \times 10^3$	$3.8 \times 10^{-3} \pm 2 \times 10^{-5}$	5.8 ± 0.9	16.4 ± 1.2	-47.0 ± 2.2	-44.6 ± 2.4	-2.5 ± 1.9	-2.9 ± 0.5
Nb6-EGF	$8.8 \times 10^5 \pm 3 \times 10^4$	$2.2 \times 10^{-2} \pm 8 \times 10^{-4}$	24.3 ± 4.1	30.3 ± 5.3	-43.5 ± 1.4	-78.7 ± 1.4	35.2 ± 1.4	-3.2 ± 0.3

^a by means of kinetic fitting; ^b steady-state or equilibrium fitting.

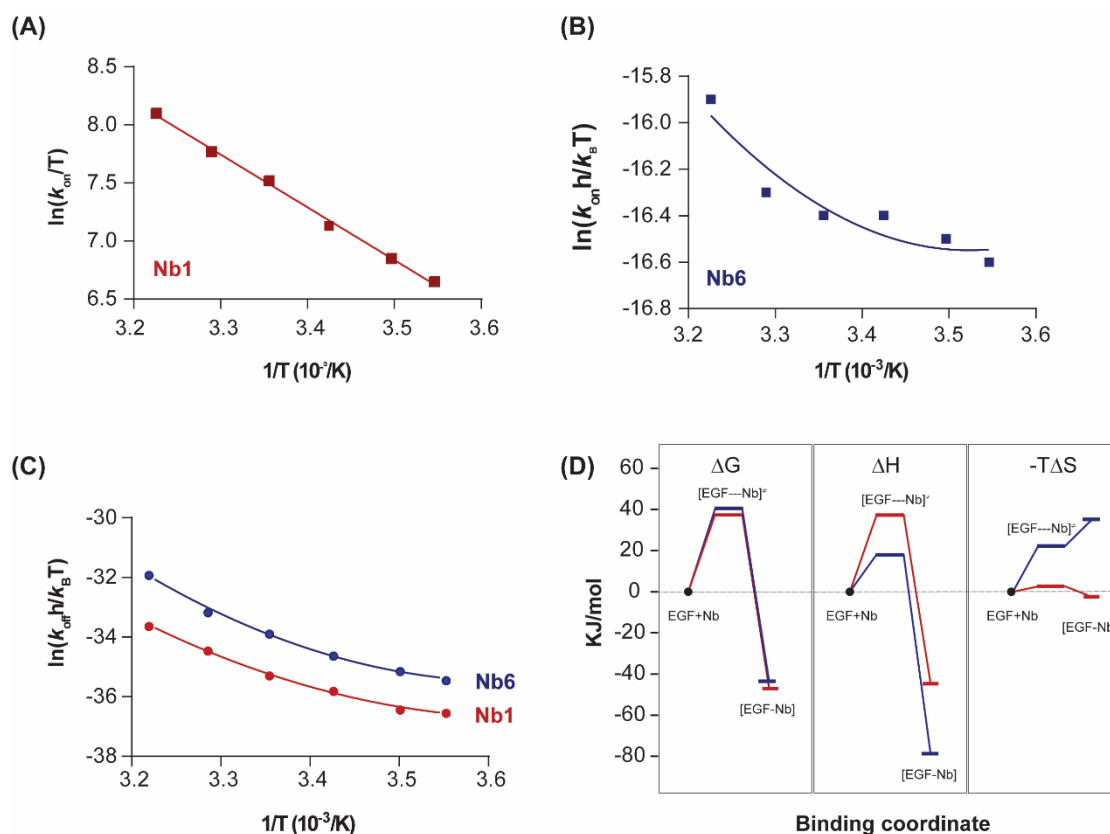


Figure 3. Transition state thermodynamics analysis. (A,B) Eyring plots representing the variation of the association constant (k_{on}) with the inverse of temperature for Nb1 and Nb6. Linear fitting of the experimental data points to Equation (4) ($\Delta C_p^\ddagger = 0$) was performed in (A), while non-linear fitting was performed in (B). (C) Eyring plots for the dissociation step of Nb1 and Nb6. Data were fitted to a second-order polynomial from which the transition state thermodynamic parameters were derived according to Equation (4). (D) Binding profile of Nb1 and Nb6 illustrating the transitions in ΔG , ΔH , ΔS at 25 °C. $[EGF-Nb]^\ddagger$ represents the transition state.

3. Discussion

From a biophysical point of view, the analysis of Ab–Ag interactions is often limited to the determination of their binding affinity values. These are sometimes complemented with predictive computational models or high-resolution crystallographic data of the complex. However, the roles of kinetics and thermodynamics in Ab–Ag molecular recognition are frequently overlooked, and this is especially the case for the newer types of antibody formats such as single-chain Abs or nanobodies. However, drawing an analogy with the rational design of small-molecule drugs, it is widely acknowledged that a more detailed notion of the molecular forces driving the interaction is essential to fully understand the binding mechanism of the drug and thus be able to implement rational changes to improve their biological efficacy [28].

Here, we have interrogated the kinetics and thermodynamics of two anti-EGF nanobodies by means of surface plasmon resonance (SPR), a technique that is widely implemented in research laboratories to determine binding affinities. This approach combines high sensitivity and throughput (it can be readily automated for 96- or 384-microwell formats) with low sample consumption and no need of labels for the ligand or the analyte, thus allowing the kinetic and thermodynamic profiling of a large number of preclinical Ab candidates.

Our results show that, for both nanobodies, the formation of the EGF-Ab complex is characterised by negative changes in enthalpy ΔC and heat capacity ΔC_p (Figure 2D and Table 1), which are caused by the formation of specific contacts between the two molecules, such as hydrogen bonds and electrostatic interactions, and might be accompanied by the burial of hydrophobic surface patches (negative ΔC_p). Furthermore, in contrast to Nb6, binding entropy is favourable for Nb1, which, together with its extended on-target residence time, might support its development for potential clinical use.

A key differential feature is the much higher entropy penalty of Nb6 in comparison with Nb1, a difference that already arises in the association step towards the transition state (ΔS^\ddagger), and which is likely to derive from conformational adjustments of the hypervariable loops at the nanobody binding interface (Figure 3C). The impact of these distinct energetic profiles on the kinetic behaviour of each nanobody (fast off-rate k_{off} for Nb6, slow for Nb1) remains an open question. A plausible explanation for this difference, derived from the Eyring analysis of the Nb1 transition state, is that the large dissociation activation enthalpy ($\Delta H^\ddagger = 82.4$ kJ/mol) acts as an energetic barrier, preventing the unbinding of Nb1 from the complex once it has formed. Further investigations are nevertheless required.

4. Materials and Methods

Recombinant human EGF (MW = 6.2 kDa) was expressed as previously described [21] and was immobilised by amine coupling onto a CM5 sensor chip (series S) using the Biacore T200 (Cytiva, formerly GE Healthcare Life Sciences, Marlborough, MA, USA) at 25 °C. Three different flow cells were independently activated using the regular ratio 1:1 of a 0.4 M 1-ethyl-3-(3-dimethylaminopropyl)-carbodiimide (EDC) and a 0.1 M *N*-hydroxysuccinimide (NHS) for 7 min at 15 μ L/min and phosphate buffer saline (PBS) as running buffer. The ligand (EGF) was then injected at 1.87 μ M in 10 mM acetate buffer pH 4 in channel 2 and 4 in order to achieve 100 and 50 RU, respectively. Considering the size of the SPR chip (0.5×2.9 mm = 1.45 mm²), the channel surface is 0.36 mm². Since 1 RU \approx 1 pg/mm², approximately [29], this results in \approx 138 pg of EGF in our low-density channel, while for the high-density channel, \approx 275 pg of EGF were immobilised (these numbers compare well with the reported EGF concentration in biological media—human serum EGF is 300–800 pg/mL [30]). The reference channel (flow cell 1) was treated in the same way but with no ligand (EGF) injected. Finally, channels 1, 2 and 4 were blocked using ethanolamine 1 M pH 8.5 for 7 min at 15 μ L/min. Channel 3 was left unmodified. Nanobodies were freshly expressed as previously described [19] and used within 1 month of storage at 4 °C, to avoid aggregation artifacts. For affinity, kinetics and thermodynamics experiments, Tween-20 (0.05%) was added to the PBS running buffer.

Kinetic and affinity experiments were performed at 25 °C using a multicycle method, consisting of short regeneration periods (30 s at 30 μ L/min of 50 mM HCl) after each analyte injection. Nanobodies were serially diluted at a range of concentrations (75 to 5 nM for Nb1, and 100 to 10 nM, for Nb6) and were injected as analytes for 120 s (followed by 120 s of dissociation) at 30 μ L/min. Both high- and low-density channels were combined for global kinetic fittings (see Supporting Data 1 to 3). Thermodynamic studies were performed at a range of temperatures—9, 13, 19, 25, 31, and 37 °C—on the ligand high-density channel. All experiments were performed in duplicate. The resulting sensorgrams were double referenced and fitted to 1:1 Langmuir binding model using Biacore T200 Evaluation Software version 3.1.

Determination of the kinetic and thermodynamic parameters was performed as described below, by fitting the data to Equations (3) and (4) using GraphPad Prism 8 software (see Supporting Data 4

to 7). In Equations (1)–(4), K_D is the affinity constant (also equilibrium dissociation constant), K_A is the equilibrium association constant, k_{on} and k_{off} are the kinetic association and dissociation constants, respectively. ΔG° , ΔH° , ΔS° and ΔC_p° are the Gibbs free energy, enthalpy, entropy and heat capacity changes under standard conditions (the superscript “ $^\circ$ ” denotes the standard state: 1 atm and 298.15 K; while “ ‡ ” refers to the transition state). In Eyring’s equation Equation (4), k_B is Boltzmann’s constant (1.381×10^{-23} J K $^{-1}$) and h is Plank’s constant (6.626×10^{-34} J s).

5. Conclusions

Our results demonstrate that a comprehensive Ab–Ag interaction analysis, based on thermodynamic and kinetic parameters, can be obtained in a straightforward manner from an SPR biosensor setup. This methodology will prove to be valuable for identifying the underlying structural, thermodynamic and kinetic clues employed by nature-evolved antibodies to recognise their cognate antigens. In addition, since mAb and other Ab formats have currently become one of the most important classes of pharmaceutical agents, we believe that this type of mechanistic analysis will enable researchers to rationally design and engineer improved antibodies with higher affinity, specificity and biochemical stability.

Supplementary Materials: The following are available online at <http://www.mdpi.com/1424-8247/13/6/134/s1>, Figure S1: SPR equilibrium responses of Nb1 (A) and Nb6 (B) at a range of concentrations. K_D values resulting from non-linear curve fitting to a 1:1 Langmuir model are reported in Table 1 (main text).; Figure S2: Semilogarithmic plots of the dissociation phases for Nb1 (A) and Nb6 (B) at 50 nM over a range of temperatures, indicating that dissociation largely follows first-order kinetics at each temperature (note the exception for Nb6 at 37 °C, with a very fast dissociation that deviates from linearity).

Author Contributions: Data curation, M.V. and M.T.; Formal analysis, M.D.-L.; Funding acquisition, E.G.; Investigation, S.G.; Methodology, S.G., M.T. and J.G.; Validation, M.V., J.G. and E.G.; Writing—original draft, S.G.; Writing—review & editing, M.V., M.T., M.D.-L., J.G. and E.G. All authors have read and agreed to the published version of the manuscript.

Funding: This study was funded by MINECO-FEDER (BIO 2016-75327-R) and the Generalitat de Catalunya (XRB and 2017SGR-998).

Acknowledgments: We thank Antoni Berenguer (Biostatistics and Bioinformatics Unit, IRB Barcelona) and Néstor Santiago (Cytiva) for their technical support. We also acknowledge the computer resources at Mare Nostrum and the technical support provided by the Barcelona Supercomputing Center (BCV-2018-1-0005). IRB Barcelona is the recipient of a Severo Ochoa Award of Excellence from MINECO (Government of Spain). Mass Spectrometry and Proteomics Core Facility actively participates in the BMBS European COST Action BM 1403 and is a member of Proteored, PRB3-ISCI, supported by grant PRB3 (IPT17/0019-ISCI-SGEFI/ERDF).

Conflicts of Interest: The authors declare no conflict of interest.

References

1. Flajnik, M.F.; Kasahara, M. Origin and evolution of the adaptive immune system: Genetic events and selective pressures. *Nat. Rev. Genet.* **2010**, *11*, 47–59. [[CrossRef](#)]
2. Schroeder, H.W. The evolution and development of the antibody repertoire. *Front. Immunol.* **2015**, *6*, 33. [[CrossRef](#)]
3. Freise, A.C.; Wu, A.M. In vivo imaging with antibodies and engineered fragments. *Mol. Immunol.* **2015**, *67*, 142–152. [[CrossRef](#)] [[PubMed](#)]
4. Zolot, R.S.; Basu, S.; Million, R.P. Antibody-drug conjugates. *Nat. Rev. Drug Discov.* **2013**, *12*, 259–260. [[CrossRef](#)] [[PubMed](#)]
5. Borrebaeck, C.A.K. Antibodies in diagnostics—From immunoassays to protein chips. *Immunol. Today* **2000**, *21*, 379–382. [[CrossRef](#)]
6. Lu, R.M.; Hwang, Y.C.; Liu, I.J.; Lee, C.C.; Tsai, H.Z.; Li, H.J.; Wu, H.C. Development of therapeutic antibodies for the treatment of diseases. *J. Biomed. Sci.* **2020**, *27*, 1–30. [[CrossRef](#)] [[PubMed](#)]
7. Chames, P.; Van Regenmortel, M.; Weiss, E.; Baty, D. Therapeutic antibodies: Successes, limitations and hopes for the future. *Br. J. Pharmacol.* **2009**, *157*, 220–233. [[CrossRef](#)]

8. Bradbury, A.R.M.; Sidhu, S.; Dübel, S.; McCafferty, J. Beyond natural antibodies: The power of in vitro display technologies. *Nat. Biotechnol.* **2011**, *29*, 245–254. [[CrossRef](#)]
9. Chiu, M.L.; Gilliland, G.L. Engineering antibody therapeutics. *Curr. Opin. Struct. Biol.* **2016**, *38*, 163–173. [[CrossRef](#)]
10. Hamers-Casterman, C.; Atarhouch, T.; Muyldermans, S.; Robinson, G.; Hammers, C.; Songa, E.B.; Bendahman, N.; Hammers, R. Naturally occurring antibodies devoid of light chains. *Nature* **1993**, *363*, 446–448. [[CrossRef](#)]
11. Vincke, C.; Gutiérrez, C.; Wernery, U.; Devoogdt, N.; Hassanzadeh-Ghassabeh, G.; Muyldermans, S. Generation of Single Domain Antibody Fragments Derived from Camelids and Generation of Manifold Constructs. In *Methods in Molecular Biology (Clifton, NJ, USA)*; Humana Press: Totowa, NJ, USA, 2012; Volume 907, pp. 145–176.
12. Henry, K.A.; MacKenzie, C.R. Antigen recognition by single-domain antibodies: Structural latitudes and constraints. *MAbs* **2018**, *10*, 815–826. [[CrossRef](#)] [[PubMed](#)]
13. Sundberg, E.J.; Mariuzza, R.A. Molecular recognition in antibody-antigen complexes. *Adv. Protein Chem.* **2002**, *61*, 119–160. [[PubMed](#)]
14. Akiba, H.; Tsumoto, K. Thermodynamics of antibody—Antigen interaction revealed by mutation analysis of antibody variable regions. *J. Biochem.* **2015**, *158*, 1–13. [[CrossRef](#)]
15. Akiba, H.; Tamura, H.; Kiyoshi, M.; Yanaka, S.; Sugase, K.; Caaveiro, J.M.M.; Tsumoto, K. Structural and thermodynamic basis for the recognition of the substrate-binding cleft on hen egg lysozyme by a single-domain antibody. *Sci. Rep.* **2019**, *9*. [[CrossRef](#)] [[PubMed](#)]
16. Adhikary, R.; Yu, W.; Oda, M.; Zimmermann, J.; Romesberg, F.E. Protein dynamics and the diversity of an antibody response. *J. Biol. Chem.* **2012**, *287*, 27139–27147. [[CrossRef](#)]
17. Sagawa, T.; Oda, M.; Ishimura, M.; Furukawa, K.; Azuma, T. Thermodynamic and kinetic aspects of antibody evolution during the immune response to hapten. *Mol. Immunol.* **2003**, *39*, 801–808. [[CrossRef](#)]
18. Garbett, N.C.; Chaires, J.B. Thermodynamic studies for drug design and screening. *Expert Opin. Drug Discov.* **2012**, *7*, 299–314. [[CrossRef](#)]
19. Guardiola, S.; Varese, M.; Sánchez-Navarro, M.; Vincke, C.; Teixidó, M.; García, J.; Muyldermans, S.; Giral, E. Blocking EGFR Activation with Anti-EGF Nanobodies via Two Distinct Molecular Recognition Mechanisms. *Angew. Chemie Int. Ed.* **2018**, *57*, 13843–13847. [[CrossRef](#)]
20. Troiani, T.; Napolitano, S.; Della Corte, C.M.; Martini, G.; Martinelli, E.; Morgillo, F.; Ciardiello, F. Therapeutic value of EGFR inhibition in CRC and NSCLC: 15 years of clinical evidence. *ESMO Open* **2016**, *1*, e000088. [[CrossRef](#)]
21. Guardiola, S.; Díaz-Lobo, M.; Seco, J.; García, J.; Nevola, L.; Giral, E. Peptides Targeting EGF Block the EGF-EGFR Interaction. *ChemBioChem* **2016**, *17*, 702–711. [[CrossRef](#)]
22. Domagala, T.; Konstantopoulos, N.; Smyth, F.; Jorissen, R.N.; Fabri, L.; Geleick, D.; Lax, I.; Schlessinger, J.; Sawyer, W.; Howlett, G.J.; et al. Stoichiometry, kinetic and binding analysis of the interaction between epidermal growth factor (EGF) and the extracellular domain of the EGF receptor. *Growth Factors* **2000**, *18*, 11–29. [[CrossRef](#)] [[PubMed](#)]
23. Schuck, P.; Zhao, H. The role of mass transport limitation and surface heterogeneity in the biophysical characterization of macromolecular binding processes by SPR biosensing. *Methods Mol. Biol.* **2010**, *627*, 15–54.
24. Tuñón, I.; Silla, E.; Pascual-Ahuir, J.L. Molecular surface area and hydrophobic effect. *Protein Eng. Des. Sel.* **1992**, *5*, 715–716. [[CrossRef](#)] [[PubMed](#)]
25. Stites, W.E. Protein-protein interactions: Interface structure, binding thermodynamics, and mutational analysis. *Chem. Rev.* **1997**, *97*, 1233–1250. [[CrossRef](#)]
26. Laidler, K.J.; King, M.C. The development of transition-state theory. *J. Phys. Chem.* **1983**, *87*, 2657–2664. [[CrossRef](#)]
27. Willcox, B.E.; Gao, G.F.; Wyer, J.R.; Ladbury, J.E.; Bell, J.I.; Jakobsen, B.K.; Van der Merwe, P.A. TCR binding to peptide-MHC stabilizes a flexible recognition interface. *Immunity* **1999**, *10*, 357–365. [[CrossRef](#)]
28. Varese, M.; Guardiola, S.; García, J.; Giral, E. Enthalpy-versus Entropy-Driven Molecular Recognition in the Era of Biologics. *ChemBioChem* **2019**, *20*, 2981–2986. [[CrossRef](#)]

29. Stenberg, E.; Persson, B.; Roos, H.; Urbaniczky, C. Quantitative determination of surface concentration of protein with surface plasmon resonance using radiolabeled proteins. *J. Colloid Interface Sci.* **1991**, *143*, 513–526. [[CrossRef](#)]
30. Joh, T.; Itoh, M.; Katsumi, K.; Yokoyama, Y.; Takeuchi, T.; Kato, T.; Wada, Y.; Tanaka, R. Physiological concentrations of human epidermal growth factor in biological fluids: Use of a sensitive enzyme immunoassay. *Clin. Chim. Acta* **1986**, *158*, 81–90. [[CrossRef](#)]



© 2020 by the authors. Licensee MDPI, Basel, Switzerland. This article is an open access article distributed under the terms and conditions of the Creative Commons Attribution (CC BY) license (<http://creativecommons.org/licenses/by/4.0/>).